

Crystals and liquid crystals confined to curved geometries

Vinzenz Koning and Vincenzo Vitelli

Instituut-Lorentz, Universiteit Leiden, 2300 RA Leiden, The Netherlands

Abstract

This review introduces the elasticity theory of two-dimensional crystals and nematic liquid crystals on curved surfaces, the energetics of topological defects (disclinations, dislocations and pleats) in these ordered phases, and the interaction of defects with the underlying curvature. This chapter concludes with two cases of three-dimensional nematic phases confined to spaces with curved boundaries, namely a torus and a spherical shell.

CONTENTS

I. Introduction	3
II. Crystalline solids and liquid crystals	5
III. Differential geometry of surfaces	6
A. Preliminaries	6
B. Curvature	8
C. Monge gauge	10
IV. Elasticity on curved surfaces and in confined geometries	10
A. Elasticity of a two-dimensional nematic liquid crystal	10
B. Elasticity of a two-dimensional solid	12
C. Elasticity of a three-dimensional nematic liquid crystal	14
V. Topological defects	14
A. Disclinations in a nematic	15
B. Disclinations in a crystal	15
C. Dislocations	17
VI. Interaction between curvature and defects	17
A. Coupling in liquid crystals	17
B. Coupling in crystals	19
C. Screening by dislocations and pleats	20
D. Geometrical potentials and forces	20
VII. Nematics in spherical geometries	22
A. Nematic order on the sphere	22
B. Beyond two dimensions: spherical nematic shells	23
VIII. Toroidal nematics	25
IX. Concluding remarks	26
References	27

I. INTRODUCTION

Whether it concerns biological matter such as membranes, DNA and viruses, or synthesised anisotropic colloidal particles, the deformations inherent to soft matter almost inevitably call for a geometric description. Therefore, the use of geometry has always been essential in our understanding of the physics of soft matter. However, only recently geometry has turned into an instrument for the design and engineering of micron scaled materials. Key concepts are geometrical frustration and the topological defects that are often a consequence of this frustration [1–3].

Geometrical frustration refers to the impossibility of local order to propagate throughout a chosen space. This impossibility is of geometric nature and could for instance be due to the topology of the space. Probably your first and most familiar encounter with this phenomenon was while playing (association) football. The mathematically inclined amongst you may have wandered off during the game and wondered: “Why does the ball contain hexagonal *and* pentagonal panels?” The ball cannot merely contain hexagonal panels: a perfect tiling of hexagons (an example of local order) cannot be achieved on the spherical surface (the space considered). There exists a constraint on the number of faces, F , edges, E , and vertices, V . The constraint is named after Euler and reads [4]

$$F - E + V = \chi, \tag{1}$$

where χ is the Euler characteristic. The Euler characteristic is a quantity insensitive to continuous deformations of the surface of the ball such as twisting and bending. We call such quantities topological. Only if one would perform violent operations such as cutting a hole in the sphere and glueing a handle to the hole a surface of differently topology can be created [4, 5]. For a surface with one handle $\chi = 0$, just as for a torus or a coffee mug. The Euler characteristic χ equals 2 for the spherical surface of the ball. Thus, Euler’s polyhedral formula (eq. (1)) ensures the need of 12 pentagonal patches besides the hexagonal ones, no matter how well inflated the ball is. To see this, write the number of faces F as the sum of the number of hexagons, H , and pentagons, P , i.e. $F = H + P$. One edge is shared by two faces, hence $E = \frac{1}{2}(6H + 5P)$. Moreover, each vertex is shared among three faces, hence $V = \frac{1}{3}(6H + 5P)$. Substituting the expressions for F , E and V into eq. (1) yields $P = 12$. These pentagons are the defects. Similarly, protein shells of spherical viruses which enclose the genetic material consist of pentavalent and hexavalent subunits [6, 7]. Another condensed

matter analog of the geometrical frustration in footballs is the ‘colloidosome’. Colloidosomes are spherical colloidal crystals [8–10] that are of considerable interest as microcapsules for delivery and controlled release of drugs [8].



FIG. 1: *Left panel:* Geometric frustration in a football. A perfect tiling of hexagonal panels cannot be achieved everywhere, resulting in black pentagonal panels (defects). *Right panel:* Geometric frustration on the globe. The lines of latitude shrink to a point at the north and south poles (defects). Adapted from http://commons.wikimedia.org/wiki/File:Latitude_lines.

Another macroscopic example of geometrical frustration are the lines of latitude on the surface of a globe. The points where these lines shrink to a point, that is the North and South Poles, are the defects. Just like the pentagons on the football the defects on the globe are also required by a topological constraint, namely the Poincare-Hopf theorem [5]:

$$\sum_a s_a = \chi. \quad (2)$$

The lines of latitude circle once around both poles. Hence, there are two defects with an unit winding number, s . (See section V for a more precise definition.) Similar to the lines of longitude and latitude on the globe, a coating of a nanoparticle with a monolayer of ordered tilted molecules also has two polar defects [11–15]. Recently, Stellacci and co-workers have been able to functionalise the defects to assemble linear chains of nanoparticles [15]. A nematic liquid crystal coating possesses four defects at the vertices of a regular tetrahedron in the ground state [12]. Attaching chemical linkers to these defects could result in a three-dimensional diamond structure [13], rather than a one-dimensional chain. This defect arrangement has been recently observed in nematic double emulsion droplets

[16], in which a nematic droplet itself contains another smaller water droplet. However, this is only one of the many defect arrangements that are observed, as the size and location of the inner water droplet is varied [16, 17]. Functionalisation of the defects, thus resulting ordered structures confined to curved surfaces or shells offers an intriguing route to directed assembly.

The types of order that we will discuss in this chapter are crystalline and (nematic) liquid crystalline. After introducing mathematical preliminaries, we will discuss the elasticity of crystals and liquid crystals and give a classification of the defects in these phases of matter. We will elucidate the role of geometry in this subject. In particular, we will explicitly show that, in contrast to the two examples given in the introduction, a topological constraint is not necessary for geometrical frustration. After that we will explore the fascinating coupling between defects and curvature. We will briefly comment on the screening by recently observed charge-neutral pleats in curved colloidal crystals. We will then cross over from a two dimensional surface to curved films with a finite thickness and variations in this thickness. The particular system we are considering is a spherical nematic shell encapsulated by a nematic double emulsion droplet. We will finish this chapter with a discussion on nematic droplets of toroidal shape. Though topology does not prescribe any defects, there is frustration due to the geometric confinement.

II. CRYSTALLINE SOLIDS AND LIQUID CRYSTALS

Besides the familiar solid, liquid and gas phases, there exist other fascinating forms of matter, which display phenomena of order intermediate between conventional isotropic fluids and crystalline solids. These are therefore called liquid crystalline or mesomorphic phases [18, 19]. Let us consider the difference between a solid crystal and a liquid crystal. In a solid crystal all the constituents are located in a periodic fashion, such that only specific translations return the same lattice. Moreover, the bonds connecting neighbouring crystal sites define a discrete set of vectors which are the same throughout the system. In a crystal, there is thus both bond-orientational and translational order. In liquid crystals there is orientational order, as the anisotropic constituent molecules define a direction in space, but the translational order is partially or fully lost. The latter phase, in which there is no translational order whatsoever, is called a nematic liquid crystal. The loss of

translational order is responsible for the fluidic properties of nematic liquid crystals. A thorough introduction to liquid crystals can be found in the chapter by Lagerwall.

III. DIFFERENTIAL GEOMETRY OF SURFACES

A. Preliminaries

For a thorough introduction to the differential geometry of surfaces, please consult refs. [3, 20, 21]. In this section we will introduce the topic briefly and establish the notation. Points on a curved surface embedded in the three dimensional world we live in can be described by a three-component vector $\mathbf{R}(\mathbf{x})$ as a function of the coordinates $\mathbf{x} = (x^1, x^2)$. Vectors tangent to this surface are given by

$$\mathbf{t}_\alpha = \partial_\alpha \mathbf{R}, \quad (3)$$

where $\partial_\alpha = \frac{\partial}{\partial x^\alpha}$ is the partial derivative with respect to x^α . These are in general neither normalised nor orthogonal. However, it does provide a basis to express an arbitrary tangent vector \mathbf{n} in:

$$\mathbf{n} = n^\alpha \mathbf{t}_\alpha. \quad (4)$$

Here we have used the Einstein summation convention, *i.e.*, an index occurring twice in a single term is summed over, provided that one of the them is a lower (covariant) index and the other is an upper (contravariant) index. We reserve Greek characters $\alpha, \beta, \gamma, \dots$ as indices for components of vectors and tensors tangent to the surface. The so-called metric tensor reads

$$g_{\alpha\beta} = \mathbf{t}_\alpha \cdot \mathbf{t}_\beta. \quad (5)$$

and its inverse is defined by

$$g^{\alpha\beta} g_{\beta\gamma} = \delta_\gamma^\alpha, \quad (6)$$

where δ_γ^α is equal to one if $\alpha = \gamma$ and zero otherwise. We can lower and raise indices with the metric tensor and inverse metric tensor, respectively, in the usual way, e.g.

$$g_{\alpha\beta} n^\alpha = n_\beta \quad (7)$$

It is straightforward to see that the inner product between two vectors \mathbf{n} and \mathbf{m} is

$$\mathbf{n} \cdot \mathbf{m} = n^\alpha \mathbf{t}_\alpha \cdot m^\beta \mathbf{t}_\beta = g_{\alpha\beta} n^\alpha m^\beta = n^\alpha m_\alpha. \quad (8)$$

The area of the parallelogram generated by the infinitesimal vectors $dx^1 \mathbf{t}_1$ and $dx^2 \mathbf{t}_2$, given by the magnitude of their cross product, yields the area element

$$\begin{aligned}
dS &= |dx^1 \mathbf{t}_1 \times dx^2 \mathbf{t}_2| \\
&= \sqrt{(\mathbf{t}_1 \times \mathbf{t}_2)^2} dx^1 dx^2 \\
&= \sqrt{|\mathbf{t}_1|^2 |\mathbf{t}_2|^2 - (\mathbf{t}_1 \cdot \mathbf{t}_2)^2} dx^1 dx^2 \\
&= \sqrt{g_{11}g_{22} - g_{12}g_{21}} dx^1 dx^2 \\
&= \sqrt{g} d^2x
\end{aligned} \tag{9}$$

where $g = \det(g_{\alpha\beta})$, the determinant of the metric tensor, and d^2x is shorthand for $dx^1 dx^2$. More generally, the magnitude of the cross product of two vectors \mathbf{m} and \mathbf{n} is

$$|\mathbf{m} \times \mathbf{n}| = |\gamma_{\alpha\beta} m^\alpha n^\beta|, \tag{10}$$

which introduces the antisymmetric tensor

$$\gamma_{\alpha\beta} = \sqrt{g} \epsilon_{\alpha\beta} \tag{11}$$

where $\epsilon_{\alpha\beta}$ is the Levi-Civita symbol satisfying $\epsilon_{12} = -\epsilon_{21} = 1$ and is zero otherwise.

Since we will encounter tangent unit vectors, e.g. indicating the orientation of some physical quantity, it is convenient to decompose this vector in a set of orthonormal tangent vectors, $\mathbf{e}_1(\mathbf{x})$ and $\mathbf{e}_2(\mathbf{x})$, such that

$$\mathbf{e}_i \cdot \mathbf{e}_j = \delta_{ij} \quad \text{and} \quad \mathbf{N} \cdot \mathbf{e}_i = 0, \tag{12}$$

alternative to the basis defined in eq. 3. Here \mathbf{N} is the vector normal to the surface. We use the Latin letters i, j and k for the components of vectors expressed in this orthonormal basis. As they are locally Cartesian they do not require any administration of the position of the index. Besides the area element we need a generalisation of the partial derivative. This generalisation is the covariant derivative, D_α , the projection of the derivative onto the surface. The covariant derivative of \mathbf{n} expressed in the orthonormal basis reads in component form [3]

$$\begin{aligned}
D_\alpha n_i &= \mathbf{e}_i \cdot \partial_\alpha \mathbf{n} \\
&= \mathbf{e}_i \cdot \partial_\alpha n_j \mathbf{e}_j + \mathbf{e}_i \cdot \partial_\alpha \mathbf{e}_j n_j \\
&= \partial_\alpha n_i + \epsilon_{ij} A_\alpha n_j,
\end{aligned} \tag{13}$$

where $\epsilon_{ij}A_\alpha = \mathbf{e}_i \cdot \partial_\alpha \mathbf{e}_j$ is called the spin-connection. The final line is justified because the derivative of any unit vector is perpendicular to this unit vector. More generally, the covariant derivative of the vector \mathbf{n} along x^α is [21]

$$D_\alpha n^\beta = \partial_\alpha n^\beta + \Gamma_{\alpha\gamma}^\beta n^\gamma \quad (14)$$

where the Christoffel symbols are

$$\Gamma_{\beta\gamma}^\alpha = \frac{1}{2}g^{\alpha\delta}(\partial_\gamma g_{\beta\delta} + \partial_\beta g_{\delta\gamma} - \partial_\delta g_{\beta\gamma}). \quad (15)$$

Finally, with the antisymmetric tensor and the area element in hand we can state a useful formula in integral calculus, namely Stokes' theorem

$$\int d^2x \sqrt{g} \gamma^{\alpha\beta} D_\alpha n_\beta = \oint dx^\alpha n_\alpha. \quad (16)$$

B. Curvature

The curvature is the deviation from flatness and therefore a measure of the rate of change of the tangent vectors along the normal, or, put the other way around, a measure of the rate of change of the normal along the tangent vectors. This can be cast in a curvature tensor defined as

$$K_{\alpha\beta} = \mathbf{N} \cdot \partial_\beta \mathbf{t}_\alpha = -\mathbf{t}_\alpha \cdot \partial_\alpha \mathbf{N} \quad (17)$$

From this tensor we extract the intrinsic Gaussian curvature

$$G = \det(K_\beta^\alpha) = \frac{1}{2}\gamma^{\alpha\beta}\gamma^{\gamma\delta}K_{\alpha\beta}K_{\gamma\delta} = \kappa_1\kappa_2 \quad (18)$$

and extrinsic mean curvature

$$H = \frac{1}{2}\text{Tr}(K_\beta^\alpha) = \frac{1}{2}g^{\alpha\beta}K_{\alpha\beta} = \frac{1}{2}(\kappa_1 + \kappa_2), \quad (19)$$

where $\kappa_1 = \mathbf{N} \cdot \partial_1 \tilde{\mathbf{e}}_1$ and $\kappa_2 = \mathbf{N} \cdot \partial_2 \tilde{\mathbf{e}}_2$ are the extremal or principal curvatures, the curvature in the principal directions $\tilde{\mathbf{e}}_1$ and $\tilde{\mathbf{e}}_2$. These eigenvalues and eigenvectors can be obtained by diagonalising the matrix associated with the curvature tensor. If at a point on a surface κ_1 and κ_2 have the same sign the Gaussian curvature is positive and from the outsiders' point of view the surface curves away in the same direction whichever way you go, as is the case on tops and in valleys. In contrast, if at a point on a surface κ_1 and κ_2 have opposite

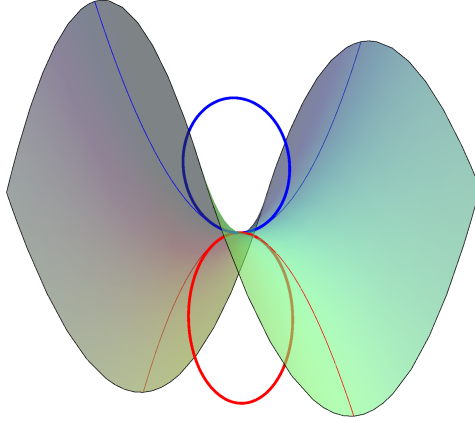


FIG. 2: Saddle surface has negative Gaussian curvature. κ_1 and κ_2 have different signs. Tangent circles are drawn in blue and red.

signs the Gaussian curvature is negative, the saddle-like surface curves away in opposite directions. The magnitude of κ_1 and κ_2 is equal to the inverse of the radius of the tangent circle in the principal direction (Fig. 2). It turns out that the Gaussian curvature and the spin-connection are related. We will see how in a moment by considering the normal (third) component of the curl (denoted by $\nabla \times$) of the spin-connection

$$\begin{aligned}
 (\nabla \times \mathbf{A})_3 &= \epsilon_{3jk} \partial_j (\mathbf{e}_1 \cdot \partial_k \mathbf{e}_2) \\
 &= \epsilon_{3jk} \partial_j \mathbf{e}_1 \cdot \partial_k \mathbf{e}_2 \\
 &= \epsilon_{3jk} (\mathbf{N} \cdot \partial_j \mathbf{e}_1) (\mathbf{N} \cdot \partial_k \mathbf{e}_2)
 \end{aligned} \tag{20}$$

where we have used the product rule and the antisymmetry of ϵ_{ijk} in the second equality sign. The final line is justified by the fact that the derivative of a unit vector is perpendicular to itself and therefore we have e.g. $\partial_j \mathbf{e}_1 = (\mathbf{N} \cdot \partial_j \mathbf{e}_1) \mathbf{N} + (\mathbf{e}_2 \cdot \partial_j \mathbf{e}_1) \mathbf{e}_2$. If we now with the aid of eqs. (18) and (17) note that

$$G = (\mathbf{N} \cdot \partial_1 \mathbf{e}_1) (\mathbf{N} \cdot \partial_2 \mathbf{e}_2) - (\mathbf{N} \cdot \partial_1 \mathbf{e}_2) (\mathbf{N} \cdot \partial_2 \mathbf{e}_1) \tag{21}$$

we easily see that the normal component of the curl of the spin-connection equals the Gaussian curvature:

$$(\nabla \times \mathbf{A}) \cdot \mathbf{N} = G, \tag{22}$$

or alternatively[22]

$$\gamma^{\alpha\beta} D_\alpha A_\beta = G. \tag{23}$$

This geometrical interpretation of \mathbf{A} will show its importance in section IV, where we will comment on its implications on the geometrical frustration in curved nematic liquid crystal films.

C. Monge gauge

A popular choice of parametrisation of the surface is the Monge gauge or height representation in which $\mathbf{x} = (x, y)$ and $\mathbf{R} = (x, y, f(x, y))$, where $f(x, y)$ is the height of the surface above the xy -plane. In this representation the Gaussian curvature reads

$$G = \frac{\det \partial_\alpha \partial_\beta f}{g}, \quad (24)$$

where the determinant of the metric is given by

$$g = 1 + (\partial_x f)^2 + (\partial_y f)^2. \quad (25)$$

IV. ELASTICITY ON CURVED SURFACES AND IN CONFINED GEOMETRIES

A. Elasticity of a two-dimensional nematic liquid crystal

In a nematic liquid crystal the molecules (assumed to be anisotropic) tend to align parallel to a common axis. The direction of this axis is labeled with a unit vector, \mathbf{n} , called the director (see Fig. 3). The states \mathbf{n} and $-\mathbf{n}$ are equivalent. Any spatial distortion of a

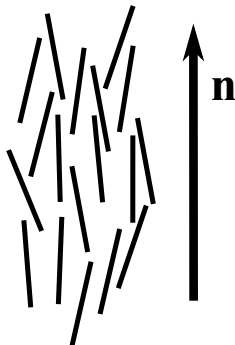


FIG. 3: The director \mathbf{n} specifies the average local orientation of the nematic molecules.

uniform director field costs energy. If we assume that these deformations are small on the molecular length scale, l ,

$$|\partial_i n_j| \ll \frac{1}{l}, \quad (26)$$

we can construct a phenomenological continuum theory. The resulting Frank free energy F for a two dimensional flat nematic liquid crystal reads [18, 23, 24]

$$F = \frac{1}{2} \int d^2x \left[k_1 (\partial_i n_i)^2 + k_3 (\epsilon_{ij} \partial_i n_j)^2 \right], \quad (27)$$

where the splay and bend elastic constants, k_1 and k_3 respectively, measure the energy of the two independent distortions shown in Fig. 4. To simplify the equations one often makes



FIG. 4: Conformations with (left panel) a non-vanishing divergence of the director and (right panel) a non-vanishing curl of the director.

the assumption of isotropic elasticity. In this approximation the Frank elastic constants are equal, $k_1 = k_3 = k$, and up to boundary terms the free energy reduces to [23]

$$F = \frac{1}{2} k \int d^2x \partial_i n_j \partial_i n_j, \quad (28)$$

When the coupling of the director to the curvature tensor $K_{\alpha\beta}$ [25–33] is ignored, the elastic free energy on a curved surface generalises to [11, 13, 14, 34, 35]

$$F = \frac{1}{2} k \int d^2x \sqrt{g} D_\alpha n^\beta D^\alpha n_\beta, \quad (29)$$

In this equation the area element has become $dS = d^2x \sqrt{g}$ and partial derivatives have been promoted to covariant derivatives. Because the director is of unit length, we can conveniently specify it in terms of its angle with a local orthonormal reference frame, $\Theta(\mathbf{x})$, as follows

$$\mathbf{n} = \cos(\Theta) \mathbf{e}_1 + \sin(\Theta) \mathbf{e}_2. \quad (30)$$

Then, since $\partial_\alpha n_1 = -\sin(\Theta) \partial_\alpha \Theta = -n_2 \partial_\alpha \Theta$ and $\partial_\alpha n_2 = \cos(\Theta) \partial_\alpha \Theta = n_1 \partial_\alpha \Theta$ we see that

$$\partial_\alpha n_i = -\epsilon_{ij} n_j \partial_\alpha \Theta \quad (31)$$

with which we find the covariant derivative to be

$$D_\alpha n_i = -\epsilon_{ij} n_j (\partial_\alpha \Theta - A_\alpha) \quad (32)$$

Therefore, we can rewrite the elastic energy as[22]

$$F = \frac{1}{2}k \int d^2x \sqrt{g} (\partial_\alpha \Theta - A_\alpha) (\partial^\alpha \Theta - A^\alpha), \quad (33)$$

where we have used that $(-\epsilon_{ij}n_j)(-\epsilon_{ij}n_j) = \delta_{jk}n_jn_k = \cos^2(\Theta) + \sin^2(\Theta) = 1$. This form of the free energy [36] clearly shows that nematic order on curved surface is geometrically frustrated. The topological constraints of the introductory section are merely a special example of the frustration of local order due to the geometrical properties of the system. Note that for a curved surface without such a topological constraint (*e.g.* a Gaussian bump) the ground state can be a deformed director field. Since the curl of the spin-connection equals the Gaussian curvature (eq. (23)), if the gaussian curvature is nonzero, the spin-connection is irrotational and cannot be written as the gradient of a scalar field, $A_\alpha \neq \partial_\alpha \Theta$, just like the magnetic field cannot be described by a scalar field either. Therefore F in eq. 33 is nonzero and we can conclude that there is geometrical frustration present in the system.

B. Elasticity of a two-dimensional solid

Similar to the construction of the continuum elastic energy of a nematic liquid crystal, we can write down the elastic energy of a linear elastic solid as an integral of terms quadratic in the deformations, *i.e.* strain. This strain is found in the following way. Consider a point $\mathbf{x} = (x, y, 0)$ on an initially flat solid. This point is displaced to $\mathbf{x}'(\mathbf{x}) = (x', y', f)$ in the deformed solid, and so we may define a displacement vector $\mathbf{u}(\mathbf{x}) = \mathbf{x}' - \mathbf{x} = u_x \mathbf{e}_x + u_y \mathbf{e}_y + f \mathbf{e}_z$. The square of the line element in the deformed plate is then given by $ds'^2 = (dx + du_x)^2 + (dy + du_y)^2 + df^2$. Noting that $du_x = \partial_i u_x dx_i$ with $x_i = x, y$ and similarly for u_y and f we find [37]

$$ds'^2 = ds^2 + 2u_{ij}dx_i dx_j. \quad (34)$$

Thus, the strain tensor $u_{ij}(\mathbf{x})$ encodes how infinitesimal distances change in the deformed body with respect to the resting state of the solid and reads

$$u_{ij} = \frac{1}{2} (\partial_i u_j + \partial_j u_i + A_{ij}), \quad (35)$$

where we have omitted non-linear terms of second order in $\partial_i u_j$ and where the tensor field $A_{ij}(\mathbf{x})$ is now defined as

$$A_{ij} \equiv \partial_i f \partial_j f. \quad (36)$$

We will assume that curvature plays its part only through this coupling of gradients of the displacement field to the geometry of the surface, and we will therefore adopt the flat space metric. This is a valid approximation for moderately curved solids, as we comment on at the end of the section [38, 39]. To leading order in gradients of the height function, A_{ij} is related to the curvature as (see eq. (24))

$$-\frac{1}{2}\epsilon_{ik}\epsilon_{jl}\partial_k\partial_l A_{ij} = \det(\partial_i\partial_j f) = G. \quad (37)$$

Isotropy of the solid leaves two independent scalar combinations of u_{ij} that contribute to the stretching energy: [37]

$$F = \frac{1}{2} \int dS (2\mu u_{ij}^2 + \lambda u_{ii}^2). \quad (38)$$

The elastic constants λ and μ called the Lamé coefficients. Minimisation of this energy with respect to u_j leads to the force balance equation:

$$\partial_i \sigma_{ij} = 0, \quad (39)$$

where the stress tensor $\sigma_{ij}(\mathbf{x})$ is defined by Hooke's law

$$\sigma_{ij} = 2\mu u_{ij} + \lambda \delta_{ij} u_{kk}. \quad (40)$$

The force balance equation can be solved by introducing the Airy stress function, $\chi(\mathbf{x})$, which satisfies

$$\sigma_{ij} = \epsilon_{ik}\epsilon_{jl}\partial_k\partial_l\chi, \quad (41)$$

since this automatically gives

$$\partial_i \sigma_{ij} = \epsilon_{jk}\partial_k [\partial_1, \partial_2] \chi = 0 \quad (42)$$

by the commutation of the partial derivatives. If one does not adopt the flat space metric, the covariant generalisation of the force balance equation is not satisfied, because the commutator of the covariant derivatives, known as the Riemann curvature tensor, does not vanish. It is actually proportional to the Gaussian curvature and indicates why the range of validity of this approach is limited to moderately curved surfaces [38, 39]. Finally, for small $\partial_i u_j$ the bond angle field, $\Theta(\mathbf{x})$, is given by

$$\Theta = \frac{1}{2}\epsilon_{ij}\partial_i u_j. \quad (43)$$

C. Elasticity of a three-dimensional nematic liquid crystal

Besides splay and bend, there are two other deformations possible in a three dimensional nematic liquid crystal. They are twist and saddle-splay, measured by elastic moduli K_2 and K_{24} . The analog of eq. (27) reads

$$F[\mathbf{n}(\mathbf{x})] = \frac{1}{2} \int dV (K_1 (\nabla \cdot \mathbf{n})^2 + K_2 (\mathbf{n} \cdot \nabla \times \mathbf{n})^2 + K_3 (\mathbf{n} \times \nabla \times \mathbf{n})^2) - K_{24} \int d\mathbf{S} \cdot (\mathbf{n} \nabla \cdot \mathbf{n} + \mathbf{n} \times \nabla \times \mathbf{n}). \quad (44)$$

The integration of the splay, twist and bend energy density is over the volume to which the nematic is confined. The saddle-splay energy per unit volume is a pure divergence term, hence the saddle-splay energy can be written as the surface integral in eq. (44). In addition to the energy in eq. (44), there is an energetic contribution coming from the interfacial interactions, often larger in magnitude. Therefore, the anchoring of the nematic molecules at the boundary can be taken as a constraint. In one of the possible anchoring conditions the director is forced to be tangential to the surface, yet free to rotate in the plane. In this case, the saddle-splay energy reduces to [40]

$$F_{24} = K_{24} \int dS (\kappa_1 n_1^2 + \kappa_2 n_2^2), \quad (45)$$

thus coupling the director to the boundary surface. We refer to the chapter by Lagerwall for a more detailed discussion on the origin of eq. (44).

V. TOPOLOGICAL DEFECTS

Topological defects are characterised by a small region where the order is not defined. Topological defects in translationally ordered media, such as crystals, are called *dislocations*. Defects in the orientational order, such as in nematic liquid crystals and again crystals, are called *disclinations*. The defects are topological when they cannot be removed by a continuous deformation of the order parameter. As we will see momentarily, they are classified according to a topological quantum number or topological charge, a quantity that may only take on a discrete set of values and which can be measured on any circuit surrounding the defect.

A. Disclinations in a nematic

Consider for concreteness a two dimensional nematic liquid crystal. A singularity in the director field is an example of a disclination. Such a point defect can be classified by its winding number, strength, or topological charge, s , which is the number of times the director rotates by 2π , when following one closed loop in counterclockwise direction around the singularity:

$$\oint d\Theta = \oint dx^\alpha \partial_\alpha \Theta = 2\pi s \quad (46)$$

We can express eq. (46) in differential form by invoking Stokes' theorem:

$$\gamma^{\alpha\beta} D_\alpha \partial_\beta \Theta = q \delta(\mathbf{x} - \mathbf{x}_a) \quad (47)$$

where we use an alternative labelling, $q = 2\pi s$, of the charge of the defect, which is located at \mathbf{x}_a . The delta-function obeys

$$\delta(\mathbf{x} - \mathbf{x}_a) = \frac{\delta(x^1 - x_a^1) \delta(x^2 - x_a^2)}{\sqrt{g}}, \quad (48)$$

such that the integral over the surface yields one. The far field contribution of the defect to the angular director in a flat plane reads

$$\Theta = s\phi + c, \quad (49)$$

as it forms a solution to the Euler-Lagrange equation of the elastic free energy

$$\partial^2 \Theta = 0. \quad (50)$$

Here, ϕ is the azimuthal angle and c is just a phase. Examples are presented in Fig. 5. Note that since the states \mathbf{n} and $-\mathbf{n}$ are equivalent, defects with half-integer strength are also possible. In fact, it is energetically favourable for an $s = 1$ defect to unbind into two $s = \frac{1}{2}$ defects [13, 41].

B. Disclinations in a crystal

Though energetically more costly, disclinations also arise in two-dimensional crystals. At these points the coordination number deviates from its ordinary value, which is six for a crystal on a triangular lattice. Just like in nematic liquid crystals, disclinations in crystals are

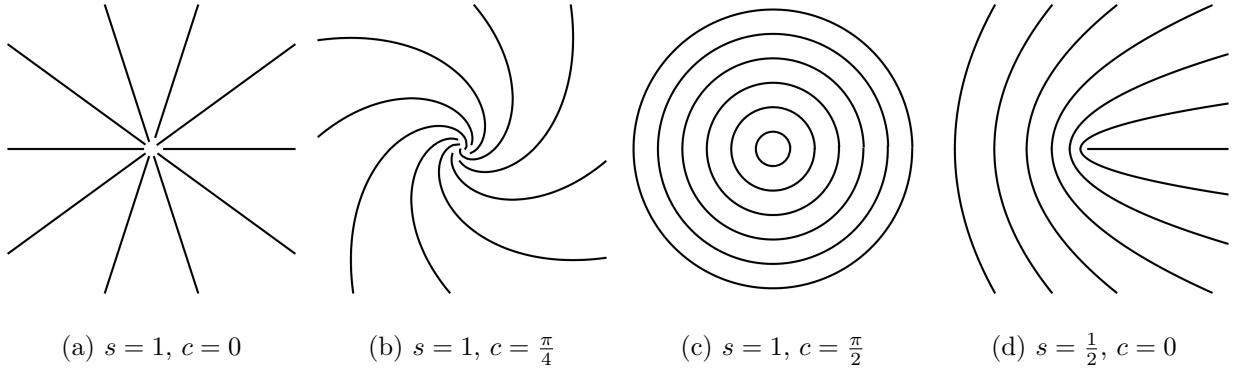


FIG. 5: Director configurations, $n_1 = \cos \Phi$, $n_2 = \sin \Phi$, for disclinations of strength s and constant c .

labelled by a topological charge, q , which is the angle over which the vectors specifying the lattice directions rotate when following a counterclockwise circuit around the disclination. If we parametrise these lattice direction vectors with $\Theta(\mathbf{x})$, the bond-angle field, this condition reads mathematically

$$\oint d\Theta = q. \quad (51)$$

Thus for disclinations in a triangular lattice with five-fold and seven-fold symmetry, as displayed in Fig. 6, $q = \frac{\pi}{3}$ and $q = -\frac{\pi}{3}$ respectively. Analogous to eq. (47), the flat-space

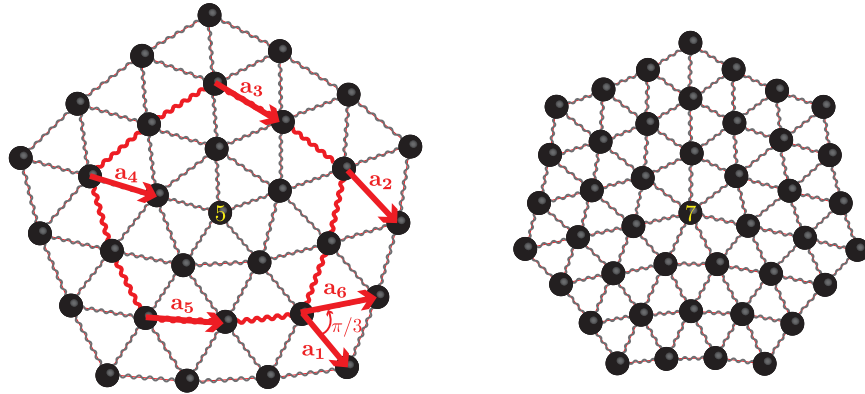


FIG. 6: (Left panel) Five-fold and (right panel) seven-fold disclination. When following a closed counterclockwise loop (red) around the five-fold disclination, the initial lattice vector \mathbf{a}_1 rotates via \mathbf{a}_2 , \mathbf{a}_3 , \mathbf{a}_4 and \mathbf{a}_5 over an angle of $\pi/3$ to \mathbf{a}_6 .

differential form of eq. (51) for a disclination located at \mathbf{x}_a reads

$$\epsilon_{ij} \partial_i \partial_j \Theta = q \delta(\mathbf{x} - \mathbf{x}_a) \quad (52)$$

C. Dislocations

Besides disclinations, dislocations can occur in crystals. Dislocations are characterised by a Burger's vector \mathbf{b} . This vector measures the change in the displacement vector, if we make a counterclockwise loop surrounding the dislocation,

$$\oint d\mathbf{u} = \mathbf{b}. \quad (53)$$

Just like the strength of disclinations can only take on a value out of a discrete set, the Burger's vector of a dislocation is equal to some integer multiple of a lattice vector. Also note that a dislocation can be viewed as a pair of closely spaced disclinations of opposite charge [42], as can be seen in Fig. 7.

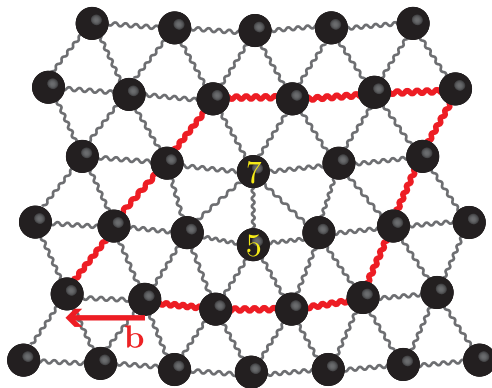


FIG. 7: Dislocation in a triangular lattice. The Burger's vector specifies by how much a clockwise circuit (marked in red, bold) around the dislocation fails to close. A dislocation can be viewed as disclination dipole with a moment perpendicular to its Burger's vector.

The flat space differential form of eq. (53) for a dislocation at \mathbf{x}_a is

$$\epsilon_{ij} \partial_i \partial_j u_k = b_k \delta(\mathbf{x} - \mathbf{x}_a), \quad (54)$$

which again can be obtained by using Stokes' theorem.

VI. INTERACTION BETWEEN CURVATURE AND DEFECTS

A. Coupling in liquid crystals

It is possible to recast the free energy in terms of the locations of the topological defects rather than the director or displacement field, if smooth (*i.e.* non-singular) deformations

are ignored. In this case the energy in eq. (33) is minimised with respect to Θ , leads to

$$D^\alpha (\partial_\alpha \Theta - A_\alpha) = 0. \quad (55)$$

This needs to be supplemented with an equation for the effective charge distribution:

$$\gamma^{\alpha\beta} D_\alpha (\partial_\beta \Theta - A_\beta) = \rho - G, \quad (56)$$

obtained by combining eq. (23) for the curvature and eq. (47) for the defect density $\rho(\mathbf{x})$,

$$\rho = \sum_a q_a \delta(\mathbf{x} - \mathbf{x}_a). \quad (57)$$

Eq. 55 is automatically satisfied if one chooses [35]

$$\partial_\alpha \Theta - A_\alpha = \gamma_\alpha^\beta \partial_\beta \chi, \quad (58)$$

where $\chi(\mathbf{x})$ is an auxiliary function. At the same time, substituting eq. (58) into eq. (56) leads to

$$-D^2 \chi = \rho - G. \quad (59)$$

The source in this Poisson equation contains both topological point charges as well as the Gaussian curvature with opposite sign. The analog of the electrostatic potential is χ . The role of the electric field is played by $\partial_\alpha \chi$. Indeed, substituting eq. (58) in eq. (33), shows that the energy density is proportional to the square of the electric field:

$$F = \frac{1}{2} k \int dS \partial_\alpha \chi \partial^\alpha \chi. \quad (60)$$

Next, we formally solve eq. (59)

$$\chi = - \int dS' \Gamma_L(\mathbf{x}, \mathbf{x}') (\rho(\mathbf{x}') - G(\mathbf{x}')) \quad (61)$$

where $\Gamma_L(\mathbf{x}, \mathbf{x}')$ is the Green function of the Laplace-Beltrami operator, $D^2 = D_\alpha D^\alpha$, satisfying

$$D^2 \Gamma_L(\mathbf{x}, \mathbf{x}') = \delta(\mathbf{x} - \mathbf{x}'). \quad (62)$$

Integrating eq.(60) by parts and substituting our expressions for χ and the Laplacian of χ (eqs. (61) and (59) respectively) results (up to boundary terms) in

$$F = -\frac{k}{2} \int dS \int dS' (\rho(\mathbf{x}) - G(\mathbf{x})) \Gamma_L(\mathbf{x}, \mathbf{x}') (\rho(\mathbf{x}') - G(\mathbf{x}')), \quad (63)$$

from which we again deduce the analogy with two-dimensional electrostatics. In this analogy the defects are electric point sources with their electric charge equal to the topological charge q and the Gaussian curvature with its sign reversed is a background charge distribution. Therefore the defects will be attracted towards regions of Gaussian curvature with the same sign as the topological charge [11, 30, 35, 43–47]. Such screening will be perfect if $S = \rho$ everywhere, since $F = 0$ then. However, unless the surface contains singularities in the Gaussian curvature, like the apex of a cone, perfect screening will be impossible, as the topological charge is quantised whereas the Gaussian curvature is typically smoothly distributed.

B. Coupling in crystals

Note that an *arbitrary* field χ solves eq. (42). However, χ must be physically possible and we therefore need to accompany eq. ((42)) with another equation, which we will obtain by considering the inversion of eq. (40) [37, 48]:

$$u_{ij} = \frac{1 + \nu}{Y} \sigma_{ij} - \frac{\nu}{Y} \sigma_{kk} \delta_{ij} \quad (64)$$

$$= \frac{1 + \nu}{Y} \epsilon_{ik} \epsilon_{jl} \partial_k \partial_l \chi - \frac{\nu}{Y} \partial^2 \chi \delta_{ij} \quad (65)$$

where the two-dimensional Young's modulus, Y , and Poisson ratio, ν , are given by

$$Y = \frac{4\mu(\mu + \lambda)}{2\mu + \lambda}, \quad (66)$$

$$\nu = \frac{\lambda}{2\mu + \lambda}. \quad (67)$$

Applying $\epsilon_{ik} \epsilon_{jl} \partial_k \partial_l$ to eq. (65) gives

$$\frac{1}{Y} \partial^4 \chi = \epsilon_{ik} \epsilon_{jl} \partial_k \partial_l u_{ij}. \quad (68)$$

By invoking eqs. (35), (43), the differential expressions for the defects, namely eqs. (54) and (52), as well as eq. (37) for the curvature, one can rewrite the right hand side to arrive at the crystalline analog of eq. (59):

$$\frac{1}{Y} \partial^4 \chi = \rho - G, \quad (69)$$

where the defect distribution, ρ , of disclinations with charge q_a and dislocations with Burger's vector \mathbf{b}^b reads

$$\rho = \sum_a q_a \delta(\mathbf{x} - \mathbf{x}_a) + \sum_b \epsilon_{ij} b_i^b \partial_j \delta(\mathbf{x} - \mathbf{x}_b). \quad (70)$$

We can also rewrite the free energy (up to boundary terms) in terms of the Airy stress function as follows:

$$F = \frac{1}{2Y} \int dS (\partial^2 \chi)^2 \quad (71)$$

If we integrate this by parts twice and use eq. (69) to eliminate χ and $\partial^4 \chi$, we find (up to boundary terms)

$$F = \frac{Y}{2} \int dS \int dS' (\rho(\mathbf{x}) - G(\mathbf{x})) \Gamma_B(\mathbf{x}, \mathbf{x}') (\rho(\mathbf{x}') - G(\mathbf{x}')) \quad (72)$$

where Γ_B is the Greens function of the biharmonic operator

$$\partial^4 \Gamma_B(\mathbf{x}, \mathbf{x}') = \delta(\mathbf{x} - \mathbf{x}'). \quad (73)$$

Eq. (72) is the crystalline analog of eq. (63). Again, the defects can screen the Gaussian curvature. The interaction, however, is different than the Coulomb interaction in the liquid crystalline case. If the surface is allowed to bend, disclinations will induce buckling, illustrated in Fig. 8 with paper models. In these cones, the integrated Gaussian curvature is determined by the angular deficit of the disclination

$$\int dS G = q. \quad (74)$$

C. Screening by dislocations and pleats

Surprisingly, also charge neutral dislocations and pleats can screen the curvature [10, 22, 38, 48, 49]. Pleats are formed by arrays of dislocations and allow for an extra piece of crystal, just like their fabric analogs. The opening angle, $\Delta\Theta$, of the pleat (or low angle grain boundary) is given by

$$\Delta\Theta \approx n_d a \quad (75)$$

where a is the lattice spacing and n_d is the dislocation line density. Since this opening angle can be arbitrarily small, pleats can provide a finer screening than quantised disclinations.

D. Geometrical potentials and forces

The cross terms of equation (72) represent the interaction energy

$$\zeta = -Y \int dS \rho(\mathbf{x}) \int dA' \Gamma_B(\mathbf{x}, \mathbf{x}') G(\mathbf{x}') \quad (76)$$

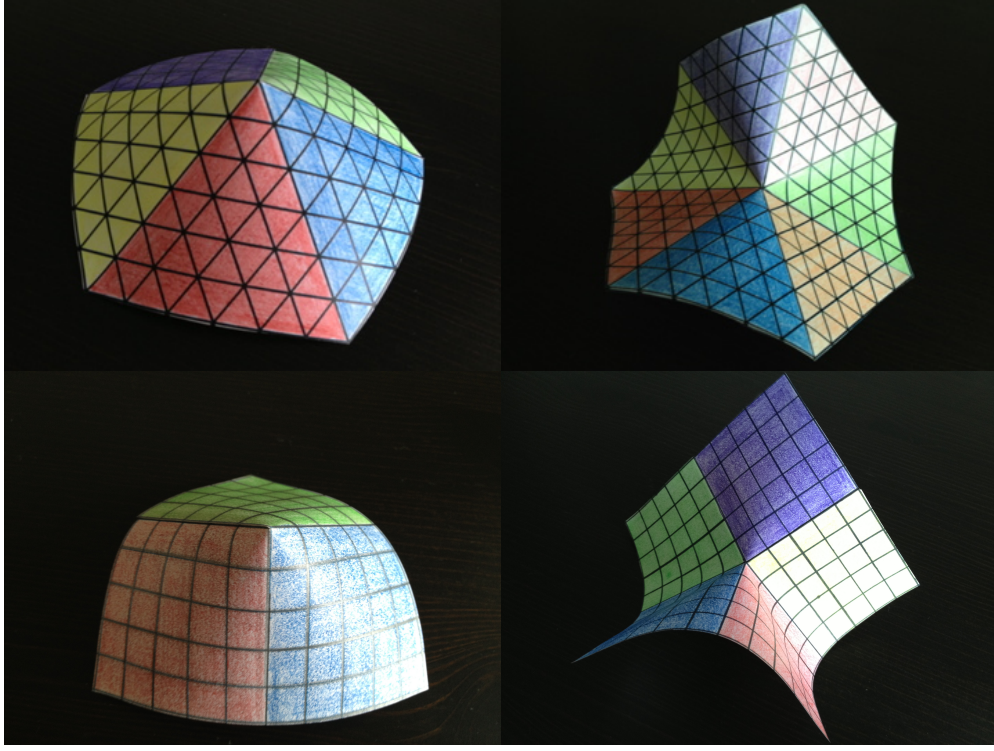


FIG. 8: Paper models illustrating the coupling between disclinations and curvature. *Left panels:* Positively (*right panels:* negatively) charged disclinations and positive (negative) Gaussian curvature attract. *Top left panel:* 5-fold coordinated particle in a triangular lattice. *Top right panel:* 7-fold coordinated particle in a triangular lattice. *Bottom left panel:* 3-fold coordinated particle in a square lattice. *Bottom right panel:* 5-fold coordinated particle in a square lattice.

By introducing an auxiliary function $V(\mathbf{x})$ satisfying

$$\partial^2 V = G, \quad (77)$$

eq. (76) can by integrating by parts twice be rewritten as

$$\zeta = -Y \int dS \rho(\mathbf{x}) \int dS' \Gamma_L(\mathbf{x}, \mathbf{x}') V(\mathbf{x}') \quad (78)$$

The field $\zeta(\mathbf{x})$ can be viewed as a geometric potential, *i.e.* the potential experienced by a defect due to the curvature of the crystal [38, 39]. Another, more heuristic way, to study the interaction of dislocations and curvature is the following. We consider the stress that exist in the monolayer as a result of curvature only, σ_{ij}^G , as the source of a Peach-Koehler

force, \mathbf{f} , on the dislocation:

$$f_k = \epsilon_{kj} b_i \sigma_{ij}^G. \quad (79)$$

Note that, by setting $\rho = 0$, the Airy stress function χ^G satisfies

$$\frac{1}{Y} \partial^4 \chi^G = -G \quad (80)$$

This equation can be solved in two steps. First, we make use of an auxiliary function U obeying

$$\partial^2 U = G \quad (81)$$

This leaves the following equation to be solved

$$\frac{1}{Y} \partial^2 \chi^G = -U + U_H, \quad (82)$$

where U_H is a harmonic function (*i.e.* $\partial^2 U_H = 0$) introduced to fulfil the boundary conditions [38].

VII. NEMATICS IN SPHERICAL GEOMETRIES

A. Nematic order on the sphere

As a naive guess for the ground state of a two dimensional nematic liquid crystal phase on the surface of the sphere, one could imagine the excess of topological charge to be located at the poles, like in the case of tilted molecules on the sphere. However, the order parameter, the director, has the symmetry of a headless arrow instead of a vector. Therefore, this makes it possible for the two $s = 1$ defects to unbind into four $s = \frac{1}{2}$ defects relaxing at the vertices of a regular tetrahedron [12]. The baseball-like nematic texture is illustrated in Fig. 9. The repulsive nature of defects with like charges can be seen from the free energy, which, as shown in the previous section, can entirely be reformulated in terms of the defects rather than the director [12, 13]:

$$F = -\frac{\pi k}{2} \sum_{i \neq j} s_i s_j \log(1 - \cos \theta_{ij}) + E(R) \sum_j s_j^2. \quad (83)$$

Here, θ_{ij} is the angular separation between defects i and j , *i.e.* $\theta_{ij} = \frac{d_{ij}}{R}$, with d_{ij} being the geodesic distance. The first term yields the long-range interaction of the charges. The



FIG. 9: The baseball-like ground state of a two-dimensional spherical nematic coating has four $s = \frac{1}{2}$ at the vertices of a tetrahedron in the one-constant approximation. Figure from [14].

second term accounts for the defect self-energy

$$E(R) = \pi k \log\left(\frac{R}{b}\right) + E_c, \quad (84)$$

where we have imposed a cut-off b representing the defect core size, which has energy E_c . This cut-off needs to be introduced in order to prevent the free energy from diverging. Heuristically, this logarithmically diverging term in the free energy is responsible for the splitting of the two $s = 1$ defects into four $s = \frac{1}{2}$ defects. Two $s = 1$ defects contribute $(2 \times 1^2) \pi k \log\left(\frac{R}{b}\right) = 2\pi k \log\left(\frac{R}{b}\right)$ to the free energy, whereas four $s = \frac{1}{2}$ defects contribute only $\left(4 \times \left(\frac{1}{2}\right)^2\right) \pi k \log\left(\frac{R}{b}\right) = \pi k \log\left(\frac{R}{b}\right)$.

In addition to this ground state, other defect structures have been observed in computer simulations [50–53]. If there is a strong anisotropy in the elastic moduli, the four defects are found to lie on a great circle rather than the vertices of a regular tetrahedron [52, 53].

B. Beyond two dimensions: spherical nematic shells

An experimental model system of spherical nematics are nematic double emulsion droplets [16, 17, 54–60]. These are structures in which a water droplet is captured by a larger nematic liquid crystal droplet, which in turn is dispersed in an outer fluid. There are some crucial differences between a two-dimensional spherical nematic and these systems. Not only is the

nematic coating of a finite thickness, this thickness can be inhomogeneous as a result of buoyancy driven displacement (or other mechanisms) of the inner droplet out of the centre of the nematic droplet.

Like point disclinations in two dimensions, there exist disclination *lines* in a three dimensional nematic liquid crystal, which are categorised in similar fashion. However, charge one lines, and integral lines in general, do not exist. Such lines lose their singular cores [61, 62] by ‘escaping in the third dimension’. In shells, such an escape leads to another type of defects, namely point defects at the interface, known as boojums (Fig. 10).

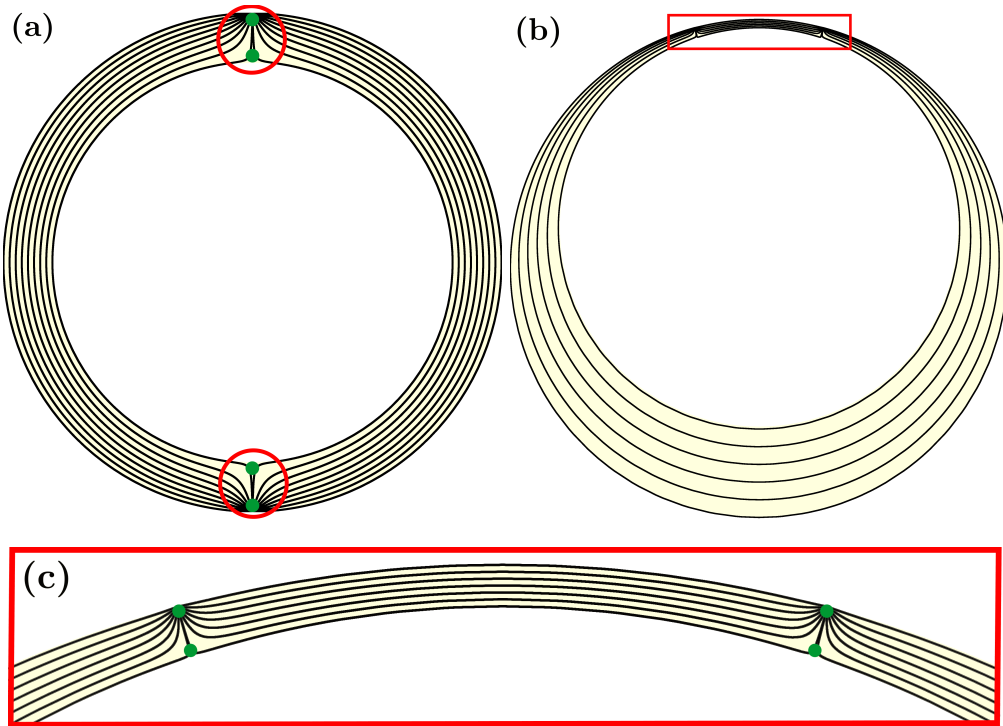


FIG. 10: (a) Schematic of the deconfined defect configuration in a homogeneous shell. Two pairs (each encircled in red) of boojums, indicated by green dots, are located at the top and bottom of the shell. (b) Schematic of the confined defect configuration in an inhomogeneous shell. All boojums are located at the thinnest, top part of the shell, inside the red rectangle. (c) Zoom of the thinnest section of the inhomogeneous shell in (b).

From [17] - Reproduced by permission of The Royal Society of Chemistry.

In a spherical nematic layer of *finite* thickness, calculations show that the baseball structure with four $s = \frac{1}{2}$ disclination lines spanning the shell, become energetically less favourable than two antipodal pairs of boojums beyond a critical thickness [14]. Instead of unbind-

ing, the singular lines escape in the third dimension, leaving two pairs of boojums on the bounding surfaces. These two defect configurations are separated by a large energy barrier. As a consequence, both configurations are observed in droplets in the same emulsion. If, in addition, the shell thickness is inhomogeneous, the energy landscape becomes even more complex.

As a consequence of the inhomogeneity the defects cluster in the thinnest part of the shell, where the length of the disclination lines (or distance between boojums forming a pair) are shorter. Since the self-energy of the disclination is proportional to its length, it is attracted towards this region of the shell. One of the intriguing outcomes of the study of inhomogeneous shells is that in the two defects shell, the pairs of surface defects can make abrupt transitions between the state in which the defects are confined in the thinnest part of the shell, and the deconfined state, in which the interdefect repulsion places them diametrically [17]. These confinement and deconfinement transitions occur when the thickness or thickness inhomogeneity is varied. A defect arrangement with a corresponding local minimum in the energy landscape makes the transition to the global minimum when the local minimum loses its stability. This explains both the abruptness of the transitions as well as the hysteresis between them.

In agreement with this picture, Monte Carlo simulations of nematic shells on uniaxial and biaxial colloidal particles have shown the tendencies for defects to accumulate in the thinnest part and in regions of the highest curvature [63].

VIII. TOROIDAL NEMATICS

The torus has a zero topological charge. Hence, in a nematic droplet of toroidal shape no defects need to be present. The director field to be expected naively in such a geometry is one which follows the tubular axis, as shown in Fig. 11. This achiral director configuration contains only bend energy. Simple analytical calculations show, however, that if the toroid becomes too fat it is favourable to reduce bend deformations by twisting. The price of twisting is screened by saddle-splay deformations provided that $K_{24} > 0$ [40, 64]. The twisted configuration is chiral. Chirality stems from the Greek word for hand, and is indeed in this context easily explained: your right hand cannot be turned into a left hand by moving and rotating it. It is only when viewed in the mirror that your right hand appears to be a left hand

and vica versa. Indeed, for small aspect ratios and small values of $(K_2 - K_{24})/K_3$ nematic toroids display either a right- or left-handedness despite the achiral nature of nematics. This phenomenon is recognised as spontaneous chiral symmetry breaking. Typical corresponding plots of the energy as a function of the amount of twist are shown in Fig. 11.

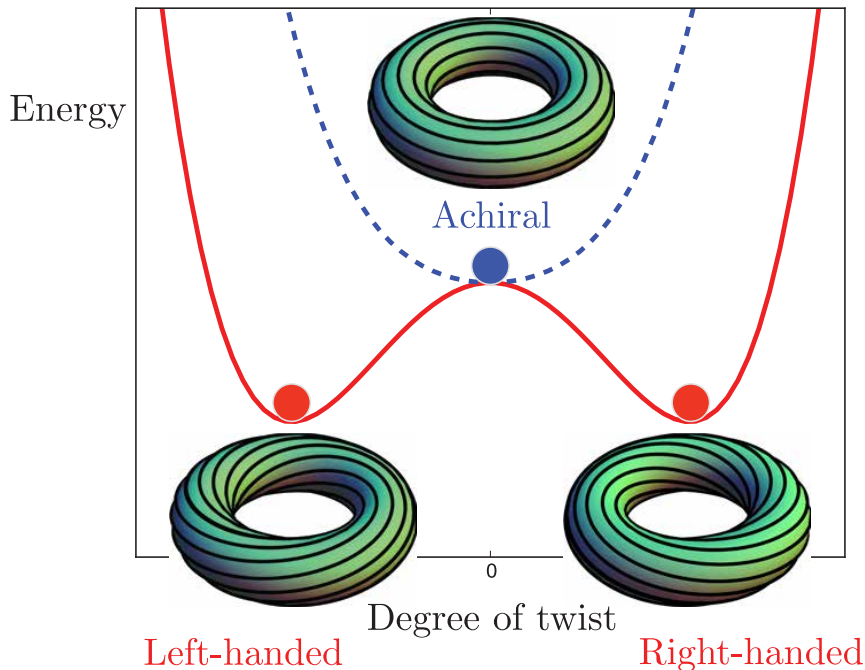


FIG. 11: Energy as a function of the degree of twist has either a single achiral minimum (dashed blue) or shows spontaneous chiral symmetry breaking in toroidal nematics (red) depending on the aspect ratio and elastic constants. The chiral state is favoured for fat toroids and small values of $(K_2 - K_{24})/K_3$.

IX. CONCLUDING REMARKS

We hope to have shared our interest in the rich subject of geometry in soft matter, in particular the interplay of defects and curvature in two-dimensional ordered matter and the confinement of nematic liquid crystals in various geometries. For readers interested in a more detailed treatment, we refer to excellent reviews by Kamien[3], Bowick and Giomi[39],

Nelson[2], David[21], and Lopez-Leon and Fernandez-Nieves [65].

- [1] J.-F. Sadoc and R. Mosseri, *Geometrical frustration* (Cambridge University Press, 2006).
- [2] D. R. Nelson, *Defects and Geometry in Condensed Matter Physics* (Cambridge University Press, 2002).
- [3] R. D. Kamien, *Rev. Mod. Phys.*, **74**, 953 (2002).
- [4] M. Monastyrsky, *Riemann, Topology, and Physics* (Birkhäuser Boston, 1999).
- [5] T. Needham, *Visual Complex Analysis* (Oxford University Press, 2000).
- [6] D. Caspar and A. Klug, *Cold Spring Harbor Symposia on Quantitative Biology*, **27**, 1 (1962).
- [7] J. Lidmar, L. Mirny, and D. R. Nelson, *Phys. Rev. E*, **68**, 051910 (2003).
- [8] A. D. Dinsmore, M. F. Hsu, M. G. Nikolaides, M. Marquez, A. R. Bausch, and D. A. Weitz, *Science*, **298**, 1006 (2002).
- [9] A. R. Bausch, M. J. Bowick, A. Cacciuto, A. D. Dinsmore, M. F. Hsu, D. R. Nelson, M. G. Nikolaides, A. Travesset, and D. A. Weitz, *Science*, **299**, 1716 (2003), arXiv:cond-mat/0303289.
- [10] W. T. M. Irvine, V. Vitelli, and P. M. Chaikin, *Nature (London)*, **468**, 947 (2010).
- [11] F. C. MacKintosh and T. C. Lubensky, *Phys. Rev. Lett.*, **67**, 1169 (1991).
- [12] T. C. Lubensky and J. Prost, *Journal de Physique II*, **2**, 371 (1992).
- [13] D. R. Nelson, *Nano Letters*, **2**, 1125 (2002), arXiv:cond-mat/0206552.
- [14] V. Vitelli and D. R. Nelson, *Phys. Rev. E*, **74**, 021711 (2006), arXiv:cond-mat/0604293.
- [15] G. A. DeVries, M. Brunnbauer, Y. Hu, A. M. Jackson, B. Long, B. T. Neltner, O. Uzun, B. H. Wunsch, and F. Stellacci, *Science*, **315**, 358 (2007).
- [16] T. Lopez-Leon, V. Koning, K. B. S. Devaiah, V. Vitelli, and A. Fernandez-Nieves, *Nature Physics*, **7**, 391 (2011).
- [17] V. Koning, T. Lopez-Leon, A. Fernandez-Nieves, and V. Vitelli, *Soft Matter*, **9**, 4993 (2013).
- [18] P. G. de Gennes and J. Prost, *The Physics of Liquid Crystals* (Oxford University Press, New York, 1993).
- [19] M. J. Stephen and J. P. Straley, *Rev. Mod. Phys.*, **46**, 617 (1974).
- [20] D. J. Struik, *Lectures on Classical Differential Geometry* (Addison Wesley Publishing Company, 1988).

- [21] F. David, *Statistical Mechanics of Membranes and Surfaces*, edited by S. W. D. Nelson, T. Piran (World Scientific, 2004) Chap. Geometry and Field Theory of Random Surfaces and Membranes.
- [22] Nelson, D.R. and Peliti, L., J. Phys. France, **48**, 1085 (1987).
- [23] M. Kléman, *Points, Lines and Walls. In Liquid Crystals, Magnetic Systems and Various Ordered Media* (John Wiley & Sons Ltd., New York, 1983).
- [24] M. Kleman and O. D. Lavrentovich, *Soft Matter Physics: An Introduction* (Springer-Verlag New York, Inc., 2003).
- [25] C. D. Santangelo, V. Vitelli, R. D. Kamien, and D. R. Nelson, Phys. Rev. Lett., **99**, 017801 (2007).
- [26] R. D. Kamien, D. R. Nelson, C. D. Santangelo, and V. Vitelli, Phys. Rev. E, **80**, 051703 (2009).
- [27] H. Jiang, G. Huber, R. A. Pelcovits, and T. R. Powers, Phys. Rev. E, **76**, 031908 (2007).
- [28] J. R. Frank and M. Kardar, Phys. Rev. E, **77**, 041705 (2008).
- [29] B. L. Mbanga, G. M. Grason, and C. D. Santangelo, Phys. Rev. Lett., **108**, 017801 (2012).
- [30] R. L. B. Selinger, A. Konya, A. Travesset, and J. V. Selinger, The Journal of Physical Chemistry B, **115**, 13989 (2011), <http://pubs.acs.org/doi/pdf/10.1021/jp205128g>.
- [31] G. Napoli and L. Vergori, Phys. Rev. Lett., **108**, 207803 (2012).
- [32] G. Napoli and L. Vergori, Phys. Rev. E, **85**, 061701 (2012).
- [33] G. Napoli and L. Vergori, International Journal of Non-Linear Mechanics, **49**, 66 (2013), ISSN 0020-7462.
- [34] J.-M. Park and T. C. Lubensky, Phys. Rev. E, **53**, 2648 (1996).
- [35] V. Vitelli and D. R. Nelson, Phys. Rev. E, **70**, 051105 (2004).
- [36] Note that if we had chosen orthonormal reference frame differing by a local rotation $\Psi(\mathbf{x})$

$$\mathbf{e}_1(\mathbf{x}) \rightarrow \cos(\Psi(\mathbf{x})) \mathbf{e}_1(\mathbf{x}) - \sin(\Psi(\mathbf{x})) \mathbf{e}_2(\mathbf{x}) \quad (85)$$

$$\mathbf{e}_2(\mathbf{x}) \rightarrow \sin(\Psi(\mathbf{x})) \mathbf{e}_1(\mathbf{x}) + \cos(\Psi(\mathbf{x})) \mathbf{e}_2(\mathbf{x}) \quad (86)$$

implying

$$\Theta(\mathbf{x}) \rightarrow \Theta(\mathbf{x}) + \Psi(\mathbf{x}) \quad A_\alpha(\mathbf{x}) \rightarrow A_\alpha(\mathbf{x}) + \partial_\alpha \Psi(\mathbf{x}) \quad (87)$$

the free energy, eq. (33), remains the same.

- [37] L. D. Landau and E. M. Lifshitz, *Theory of Elasticity*, 3rd ed., Vol. 7 (Course of Theoretical Physics) (Reed Educational and Professional Publishing Ltd., 1986).
- [38] V. Vitelli, J. B. Lucks, and D. R. Nelson, Proceedings of the National Academy of Sciences, **103**, 12323 (2006).
- [39] M. Bowick and L. Giomi, Advances in Physics, **58**, 449 (2009), arXiv:0812.3064 [cond-mat.soft].
- [40] V. Koning, B. C. van Zuiden, R. D. Kamien, and V. Vitelli, ArXiv e-prints (2013), arXiv:1312.5092 [cond-mat.soft].
- [41] T. C. L. P. M. Chaikin, *Principles of condensed matter physics* (Cambridge University Press, 1995).
- [42] D. R. Nelson and B. I. Halperin, Phys. Rev. B, **19**, 2457 (1979).
- [43] M. Bowick, D. R. Nelson, and A. Travesset, Phys. Rev. E, **69**, 041102 (2004).
- [44] V. Vitelli and A. M. Turner, Phys. Rev. Lett., **93**, 215301 (2004).
- [45] X. Xing, H. Shin, M. J. Bowick, Z. Yao, L. Jia, and M.-H. Li, Proceedings of the National Academy of Sciences, **109**, 5202 (2012).
- [46] D. Jesenek, Š. Perutková, V. Kralj-Iglič, S. Kralj, and A. Iglič, Cell Calcium, **52**, 277 (2012), ISSN 0143-4160, `jcce:title;REGULATED EXOCYSTOSIS;/ce:title;`.
- [47] S. Tie-Yan and D. Yi-Shi, Communications in Theoretical Physics, **46**, 319 (2006).
- [48] H. S. Seung and D. R. Nelson, Phys. Rev. A, **38**, 1005 (1988).
- [49] A. Hexemer, V. Vitelli, E. J. Kramer, and G. H. Fredrickson, Phys. Rev. E, **76**, 051604 (2007).
- [50] J. Dzubiella, M. Schmidt, and H. Löwen, Phys. Rev. E, **62**, 5081 (2000).
- [51] G. Skačej and C. Zannoni, Phys. Rev. Lett., **100**, 197802 (2008).
- [52] H. Shin, M. J. Bowick, and X. Xing, Phys. Rev. Lett., **101**, 037802 (2008), arXiv:0712.4012 [cond-mat.soft].
- [53] M. A. Bates, J. Chem. Phys., **128**, 104707 (2008).
- [54] A. Fernández-Nieves, V. Vitelli, A. S. Utada, D. R. Link, M. Márquez, D. R. Nelson, and D. A. Weitz, Phys. Rev. Lett., **99**, 157801 (2007).
- [55] T. Lopez-Leon and A. Fernandez-Nieves, Phys. Rev. E, **79**, 021707 (2009).
- [56] H.-L. Liang, S. Schymura, P. Rudquist, and J. Lagerwall, Phys. Rev. Lett., **106**, 247801 (2011).

- [57] T. Lopez-Leon, A. Fernandez-Nieves, M. Nobili, and C. Blanc, *Phys. Rev. Lett.*, **106**, 247802 (2011).
- [58] D. Seč, T. Lopez-Leon, M. Nobili, C. Blanc, A. Fernandez-Nieves, M. Ravnik, and S. Žumer, *Phys. Rev. E*, **86**, 020705 (2012).
- [59] H.-L. Liang, R. Zentel, P. Rudquist, and J. Lagerwall, *Soft Matter*, **8**, 5443 (2012).
- [60] H.-L. Liang, J. Noh, R. Zentel, P. Rudquist, and J. P. Lagerwall, *Philosophical Transactions of the Royal Society A: Mathematical, Physical and Engineering Sciences*, **371** (2013), doi: 10.1098/rsta.2012.0258.
- [61] P. E. Cladis, *J. Phys. France*, **33**, 591 (1972).
- [62] R. Meyer, *Philosophical Magazine*, **27**, 405 (1973).
- [63] M. A. Bates, G. Skacej, and C. Zannoni, *Soft Matter*, **6**, 655 (2010).
- [64] E. Pairam, J. Vallamkondu, V. Koning, B. C. van Zuiden, P. W. Ellis, M. A. Bates, V. Vitelli, and A. Fernandez-Nieves, *Proceedings of the National Academy of Sciences*, **110**, 9295 (2013).
- [65] T. Lopez-Leon and A. Fernandez-Nieves, *Colloid and Polymer Science*, **289**, 345 (2011), ISSN 0303-402X.